Estimation of Residual Available Capacity for Lead Acid Batteries in Electric Vehicles

W. X. Shen

School of Engineering, Monash University Malaysia, shen.wei.xiang@eng.monash.edu.my

Abstract

This paper presents a new estimation approach of residual available capacity for lead acid batteries in electric vehicles (EVs). The essence of this approach is to model lead acid batteries in EVs by using a neural network (NN) with the specially defined output and the proposed inputs. The inputs are the battery surface temperature and the discharged and regenerative capacity distribution to describe the discharge current profiles of lead acid batteries during EV operations. The output is the state of available capacity (SOAC) representing battery residual available capacity (BRAC). Then, SOACs of lead-acid batteries in EVs are experimentally investigated under different EV discharge current profiles in the presence of various battery surface temperatures. The corresponding data are recorded to train and verify the NN. The results indicate that the proposed NN can provide accurate and effective BRAC estimation for lead-acid batteries in EVs.

Keywords

electric vehicles, neural network, lead-acid batteries, battery residual available capacity

1. INTRODUCTION

In a world where environmental protection and energy conservation are growing concerns, the research and development of various technologies in electric vehicles (EVs) is being actively conducted [Chan et al.., 2002 and Chan et al., 2004]. However, the application technology of EV batteries, namely the battery residual available capacity (BRAC) indicator in EVs, can not keep pace with the development of other EV technologies. The key problem arises from highly non-linear characteristics of lead acid batteries in EVs, leading to the difficulty in the BRAC estimation and thus the driving range estimation for EVs.

Within the past three decades, the BRAC estimation for the lead-acid battery in EVs has been investigated by using different approaches as summarized in [Chan et al., 1999]. These approaches are based on (i). specific gravity [Berndt, 1997], (ii). open circuit voltage [Zhu et al., 2004 and Chiasson et al., 2005], (iii). impedance [Tenno et al., 2002 and Karden et al., 2002], (iv). ampere-hour counter [Song et al., 1994; Karden et al., 1996; Qi et al., 1996 and Caumont et al., 2000] and (v). neural network model [Yamazaki et al., 1998]. For the first three approaches, these battery parameters actually indicate only the battery state of charge (SOC), rather than the amount of ampere-hours that the battery can deliver. In other words, the SOC only exhibits the battery discharge capability. As to how much the BRAC can be really discharged, it not only depends on the battery discharge capability but also depends on the forthcoming discharge current and temperature that the battery will undergo during EV operations, and normally the later factors will have stronger influence on the BRAC than the former one. Although the higher the SOC the more the BRAC can be discharged at the same discharge current, they have no a quantitative relationship.

For the fourth approach, two methods have been adopted thus far. One method is to approximate the battery available capacity (BAC) at the fully charged state as the value $C_{ave}(t)$ based on the average discharge current [Song et al., 1994 and Karden et al., 1996]. Then, the BRAC $C_r(t)$ can be calculated by:

$$C_r(t) = C_{ave} - q(t) \tag{1}$$

$$q(t) = \int_0^t I_d(t)dt \tag{2}$$

where $q(t)$ is the discharged capacity, $I_d(t)$ is the instantaneous discharge current. The BRAC estimation by using (1) will cause an error unless the discharge current does not vary significantly. Table 1 shows a comparison of BACs under different EV discharge current profiles at the same battery surface temperature of 25°C.

Table 1 Comparison of BACs under different EV discharge current profiles

Profiles	ADC (A)	BAC (Ah)
FUDS	13.08	15.96
FHDS	13.11	25.05
ECE	13.21	13.05
JM10.15	13.12	15.43

It can be found that although the average discharge currents (ADCs) of the US federal urban driving schedule (FUDS), the US federal highway driving schedule (FHDS), the European standard reference cycle (ECE) and the Japanese mode 10.15 (JM10.15) are all approximately equal to 13 A (about the 3-hour discharge rate for the rated capacity of C_N = 40Ah), their BACs are very different. The other method is to approximate the BAC as the value C_{ref} based on the reference discharge current [Qi et al., 1996 and Caumont et al., 2000], such as the BAC for the 3-hour or 5-hour discharge rate, then the BRAC can be calculated by:

$$C_r(t) = C_{ref} - \alpha(I_d)q(t) \tag{3}$$

where $\alpha(I_d)$ is the corrective coefficient that is used to calculate the equivalent discharged capacity if the discharge current is either higher or lower than the reference discharge current. To determine the corrective coefficient, the battery has to be tested by one discharge current either individually [Qi et al., 1996] or in combination with the reference discharge current [Caumont et al., 2000] during the whole discharge period. However, the corrective coefficients calculated from these specially designed tests have ignored the influence of discharge current profile on the BAC, leading to create a significant error. Table 2 confirms this error even when the battery is under 2-step discharge current profiles at the same battery surface temperature of 25°C.

Table 2 Comparison of BACs under two-step discharge current profiles

Profiles	BAC(Ah)
8 A for first 3 h and 20 A for other 0.38 h	31.66
20 A for first 0.38 h and 8 A for other 3.17 h	33.00

Also, another drawback of this method is that the temperature can hardly be formulated in the calculation of the corrective coefficient because of the nonlinear relationship between the BAC and the temperature under different discharge currents as shown in Figure 1.

For the fifth approach, one NN with three layers has been proposed in [Yamazaki et al., 1998]. This NN has four neurons in the input layer to represent the battery terminal voltage, discharge current, temperature and internal impedance, and ten neurons in the output layer to indicate the SOC. The experimental data obtained from a particular discharge current profile are used to train

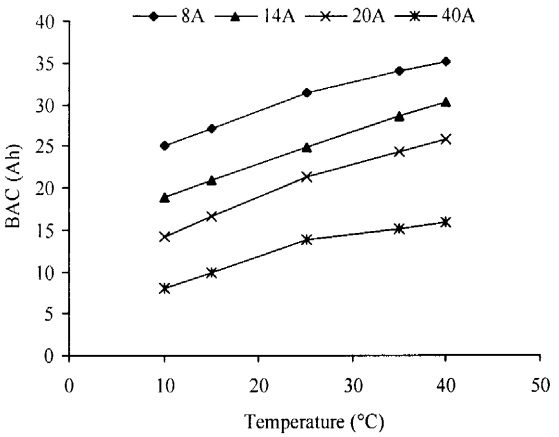

Fig. 1 Comparison of BACs under different temperatures

and verify the NN. The corresponding error is only of 10%. However, this NN has yet taken into account the discharge current profile that has strong influence on the BRAC estimation because the instantaneous terminal battery terminal voltage and discharge current are used as the inputs of the NN model to estimate the BRAC. The purpose of this paper is to propose a NN based approach that can incorporate the effect of discharge current profile into the BRAC estimation of the lead-acid battery for EVs. To achieve the goal, two technical terms are introduced. First, the state of available capacity (SOAC) $p(t)$ is specially defined to represent the BRAC, which can be written as:

$$p(t) = 1 - q(t)/C_a \tag{4}$$

where C_a refers to the BAC at the fully charged state for a discharge current profile of the battery in EVs. Second, the discharged and regenerative capacity distribution is proposed to describe the discharge current profile for the SOAC estimation. Consequently, a NN with these special inputs of the capacity distribution and the battery surface temperature is applied to estimate the SOAC (the output of the NN). Based on the experimentation under various EV discharge current profiles at different battery surface temperatures, the proposed NN model for the SOAC is established and verified.

2. EXPERIMENTATION

The NN model for the SOAC estimation requires a lot of experimental data as related to the battery in EV operations. To obtain these data, a battery evaluation and testing system is built. As shown in Figure 2, it consists of five main parts, namely a programmable battery charger, a programmable electronic load, a programmable temperature chamber, a power controller and a computer control & data acquisition subsystem. With this system, the battery can be tested under different

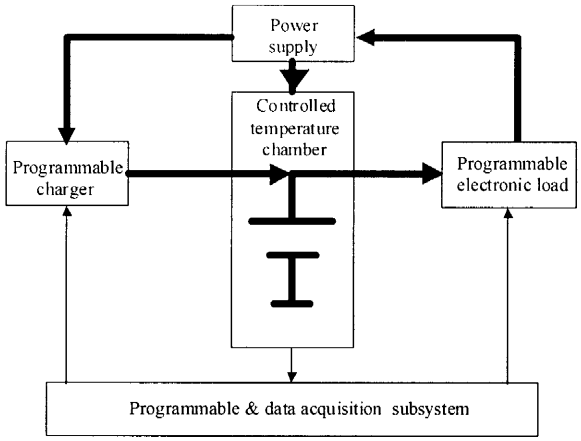

Fig. 2 Battery evaluation and testing system

charge and discharge currents at the predefined temperature.

As far as the EV battery concerned, the BAC for different discharge current profiles is the key value to govern the EV driving range. So, the discharge current profiles that emulate the battery under various EV operating conditions are designed for the BAC test:

- Constant current discharges, where each constant discharge current lies between $C_N/5$ and $C_N/1$, are used.
- Variable current discharges, where each discharge current profile has an average value approximately equal to $C_N/3$, are adopted. They can be categorized into two groups. One group is the random current discharge, including the uniform distribution discharge current with the range of $C_N/10$ to $C_N/2$ and the normal distribution discharge current with the standard deviation of $C_N/8$. Another group is the standard EV driving cycle based current discharges, including the FUDS, FHDS, ECE and JM10.15.

To carry out the BAC tests, the BAC is defined as the quantity of electricity that can be delivered by the fully charged battery at a certain discharge current profile and battery surface temperature until the specified cutoff voltage is reached. Mathematically, it can be written as:

$$C_a = f(V(t), I_d(t), T(t))\,|_{V(t)=V_{off}} \qquad (5)$$

where $V(t)$ is the battery terminal voltage, $T(t)$ is the temperature, and V_{off} is the specified cutoff voltage. With different combinations of the discharge current profiles and the temperatures ranging from 10°C to 40°C, 29 tests are carried out on the battery evaluation and testing system, where the battery at the fully charged state ($p_a(t)$ = 1) is discharged until the specified cutoff voltage of 10.8V is reached ($p_a(t)$ = 0). The experimental data are automatically recorded. From the discharged capacities for all the tests, the BACs are obtained and the corresponding SOACs can then be calculated by using (4).

Figure 3 shows two examples of the 29 tests at the temperature of 25°C, namely the discharge current profiles corresponding to the FUDS and ECE.

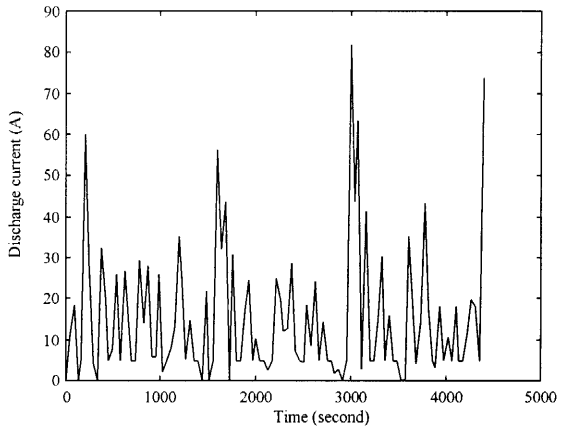

(a)

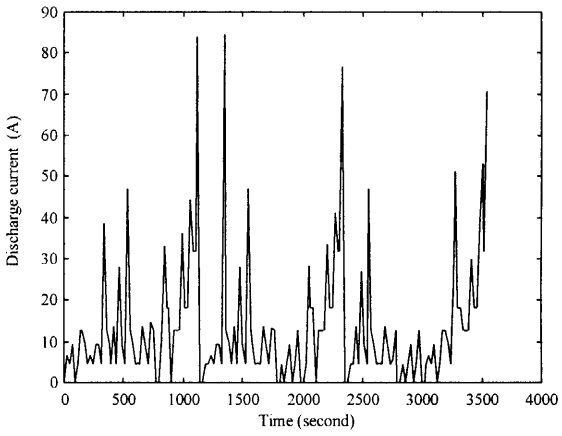

(b)

Fig. 3 Discharge current profiles of EV standard driving cycle (a) FUDS (b) ECE

3. NN MODELLING

The purpose of the NN model for the SOAC estimation is to describe the relationship between the SOAC and its related parameters. Intuitively, the SOAC has a close relationship with the instantaneous battery terminal voltage and discharge current. Due to this reason, they were chosen as the inputs of the NN for the BRAC estimation in [Yamazaki et al., 1998]. However, this is not as the case as conceived. Figure 4 illustrates the relationship between the SOAC and the battery terminal voltage, where the discharge current profiles are based on the FUDS and ECE.

It can be observed that battery terminal voltage changes considerably as a result of the significant variation of the discharge current, while the SOAC monotonously decreases with the progress of discharging. These phenomena demonstrate that the information embedded in

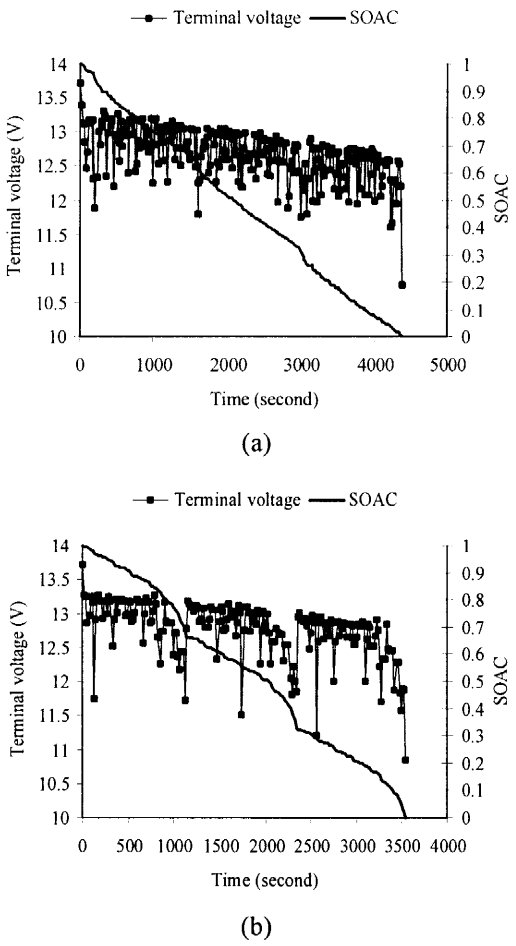

Fig. 4 Relationship between SOAC and battery terminal voltage (a) FUDS (b) ECE

the instantaneous battery terminal voltage and discharge current can not offer direct contribution to the SOAC estimation. In contrast, the BAC for the EV battery is greatly influenced by the pattern of the discharge current over time, namely the discharge current profile. Based on the experimental data, the discharged and regenerative capacity distribution is used to describe the discharge current profile for the SOAC estimation of lead acid batteries. As shown in Table 3, the discharged and regenerative capacity distribution based on the lower and upper current bounds of five current ranges, namely

Table 3 Lower and upper current bounds for discharged and regenerative capacity distribution

	i				
	1	2	3	4	5
I_i^l (A)	0	$C_N/5$	$C_N/3$	$C_N/2$	$C_N/1$
I_i^u (A)	$C_N/5$	$C_N/3$	$C_N/2$	$C_N/1$	100

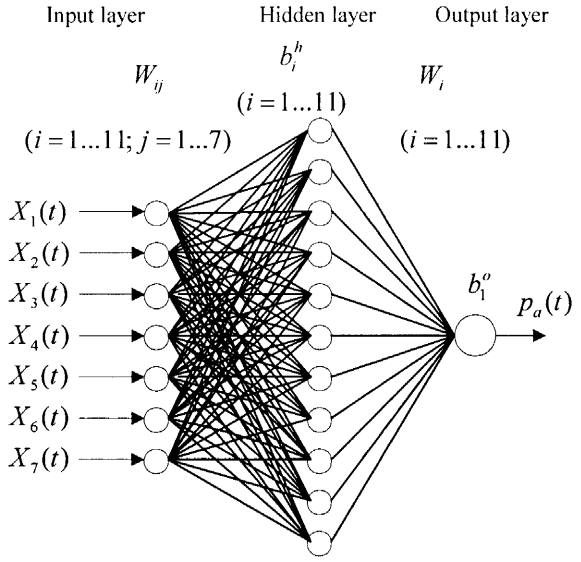

Fig. 5 NN for SOAC estimation

I_i^l and I_i^u (i = 1,...,5), is adopted. As a result, the proposed NN for the SOAC estimation is shown in Figure 5.

The NN consists of three layers. The first layer, namely the input layer, has seven neurons:

- $X_1(t)$ — discharged capacity for $I_1^l \le I_d(t) < I_1^u$;
- $X_2(t)$ — discharged capacity for $I_2^l \le I_d(t) < I_2^u$;
- $X_3(t)$ — discharged capacity for $I_3^l \le I_d(t) < I_3^u$;
- $X_4(t)$ — discharged capacity for $I_4^l \le I_d(t) < I_4^u$;
- $X_5(t)$ — discharged capacity for $I_5^l \le I_d(t) < I_5^u$;
- $X_6(t)$ — regenerative capacity for regenerative current;
- $X_7(t)$ — temperature between 10°C and 40°C.

Considering the vector $X(t) = [X_1(t)\ X_2(t)\ X_3(t)\ X_4(t)\ X_5(t)\ X_6(t)\ X_7(t)]$, the proposed NN can then be described as a function that maps the input vector $X(t)$ to the output vector $p_a(t)$, namely the SOAC at time t. Mathematically, it can be described as:

$$\hat{p}_a(t) = \sum_i^n W_i F(y_i) + b_1^o \tag{6}$$

$$F(y_i) = \frac{1-\exp(-2y_i)}{1+\exp(-2y_i)} \tag{7}$$

where $\hat{p}_a(t)$ represents the value of the SOAC estimation, n is the number of neurons in the hidden layer, W_i (i = 1,..., n) are the weights between the hidden layer and the output layer, b_1^o is the bias at the output layer, and y_i (i = 1,..., n) is the input to the i th neuron in the hidden layer. It is given by:

$$y_i = \sum_{j=1}^{7} W_{ij} X_j(t) + b_i^h \tag{8}$$

where W_{ij} (i = 1,..., n, j = 1,..., 7) are the weights between

the input layer and the hidden layer, and b_i^h (i = 1,..., n) are the biases at the hidden layer. To identify the necessary number of hidden layer neurons, eight NN candidates with n ranging from 8 to 15 are examined. Consequently, the NN with eleven hidden layer neurons is chosen because there is no significant improvement in the estimation accuracy for n greater than 11.

The learning algorithm of the NN is a numerical process that determines the connection strength, such as the weights among the layers and the biases in the neurons. In the learning process, the validation data set is included for the improvement of the generality of the NN. Under this condition, the learning process will be terminated when the error function on the validation data set begins to increase or the error function is smaller than the convergence tolerance, whichever is reached first. Here, the convergence tolerance is set at 10^{-5}. The error function E is defined as:

$$E = \frac{1}{2}\sum_{k=1}^{m}(p_a(k) - \hat{p}_a(k))^2 \qquad (9)$$

where m is the number of the training data, $p_a(k)$ is the SOAC calculated from the experimental data for the k th training data, and $\hat{p}_a(k)$ is the corresponding value of the SOAC estimated by the NN.

The parameters of this NN are optimised by the Levenberg-Marquardt algorithm, one of the improved back-propagation algorithms [Lin et al., 1996]. This algorithm is a variation of Newton's method designed for minimising functions that are sums of squares of other nonlinear functions. So, it is well suited to minimise the error function as defined in (9). With this algorithm, E can be expressed as a function of the parameters of the NN:

$$H = \left\{W_i, b_1^o, W_{ij}, b_j^h\right\} \ (i = 1,..., n, j = 1,..., 7) \qquad (10)$$

The optimum parameters of the NN can be obtained through the following iterative process:

$$H_{r+1} = H_r - A_r^{-1} g_r \qquad (11)$$

where $A_r \equiv \nabla^2 E(H)|_{H=H_r}$ and $g_r \equiv \nabla E(H)|_{H=H_r}$ are the Hessian matrix and the gradient vector of E with respect to the r th iteration, respectively.

4. RESULTS

The data obtained from the experimentation of the previous section are used to train, validate and verify the proposed NN model. Firstly, all data are normalised by the following equation:

$$X_{jn}(t) = \frac{X_j(t) - X_{j\min}}{X_{j\max} - X_{j\min}} \ (j = 1,..., 7) \qquad (12)$$

where $X_{jn}(t)$ is the normalised value, X_{jmax} and X_{jmin} are the maximum and minimum values of $X_j(t)$, respectively. After normalisation, the data for each test are collected together to form the whole data set with a total of 2505 samples, which is then grouped into the training, validation and testing data sets. The training data set is used to train the NN, the validation data set is to improve the generality of the NN while the testing data set is used to verify the accuracy and effectiveness of the trained NN for the SOAC estimation.

To allow for comparisons, the average relative percentage error (ARPE) is adopted. It is defined as:

$$ARPE = \frac{1}{N}\sum_{j=1}^{N}\frac{|p_e(j) - p_c(j)|}{|p_c(j)|}100\% \qquad (13)$$

where N is the number of the training data or the testing data for each test, p_e and p_c refer to the estimated SOAC from the trained NN and the actual SOAC calculated from the experimental data, respectively. The ARPEs for both the training data set and the testing data set for each test are calculated. Figure 6 shows the estimated SOAC and the actual SOAC for the training data set.

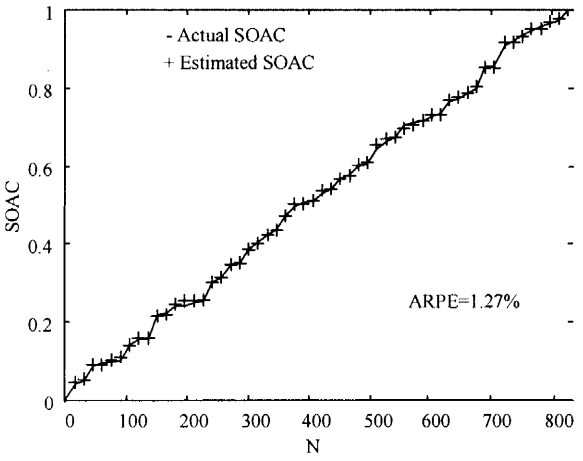

Fig. 6 Comparison between actual SOAC and estimated SOAC for training data set

It can be found that the SOAC estimation is of high accuracy and the corresponding ARPE is only of 1.27%. To testify the trained NN for the SOAC estimation effectively, the testing data for each test are used to verify the trained NN. The results corresponding to the FUDS and the ECE are of 1.31% and 1.59%, respectively (shown in Figure 7), which illustrate that the proposed

approach provides highly accurate estimation of the SOAC for different discharge current profiles. It should be noted that the ARPEs of the SOAC estimation for the aforementioned 29 tests are within 2% as summarised in Figure 8. This demonstrates that the proposed NN offers a significant improvement over the ARPEs of 10% in [Yamazaki et al., 1998], where the NNs were also adopted.

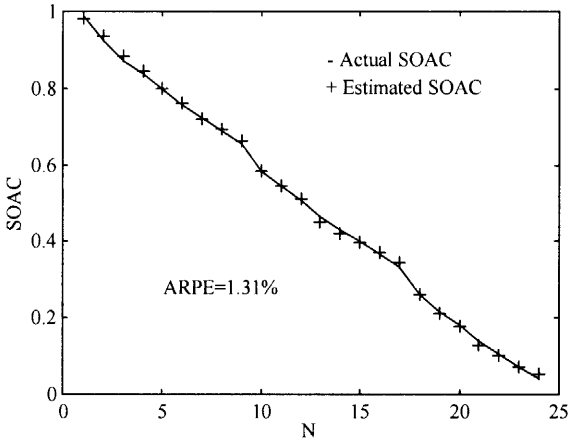

Fig. 7 Comparison between actual SOAC and estimated SOAC for testing data set (a) FUDS (b) ECE

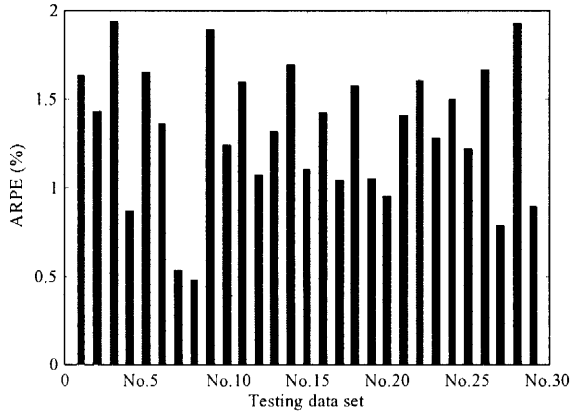

Fig. 8 ARPEs for all 29 testing data sets

5. CONCLUSIONS

In the application of a NN to the BRAC estimation of the lead-acid battery for EVs, the advancements have been made in the definition of the BRAC for the output and the selection of inputs. Their advantages have been confirmed by the experimental data of the lead-acid battery in the presence of various EV discharge current profiles at different temperatures, and can be summarised below. The SOAC, which incorporates the effects of the EV discharge current profile, is specially defined to represent the BRAC of the lead-acid battery for EVs. This definition logically follows from the fact that the BAC is strongly influenced by the EV discharge current profiles and this influence is neglected in the previous approaches. As a result, the SOAC can be used to estimate the BRAC more accurately and effectively for EVs. The specific inputs of the NN, namely the discharged and regenerative capacity distribution, are used to describe the discharge current profile. These new inputs offer the more general framework for the BRAC estimation of the EV battery. The reason is that the number of the current ranges and the values of the upper and lower current bounds, which are used to construct the capacity distribution, can be easily adjusted to adapt the complexity of the BRAC estimation for different types of EV batteries. For instance, if the experimental data of other types of EV batteries are available, the number of inputs and the hidden neurones of the NN for those batteries may be changed; however, the structure of the NN, the capacity distribution as the inputs and the algorithm can remain the same.

The NN is an emerging tool to estimate the BRAC estimation for EVs. Comparisons between the estimated SOACs and the actual SOACs demonstrate that even a simple three-layer NN can provide high accuracy of the SOAC estimation with the ARPE less than 2% for all 29 testing data sets.

References

Berndt, D., *Maintenance-free batteries: lead-acid, nickel/cadmium, nickel/metal hydride: a handbook of battery technology*, Research Studies Press, 1997.

Caumont, O., P. L. Moigne, C. Rombaut, X. Muneret, and P. Lenain, Energy gauge for lead acid batteries in electric vehicles, *IEEE Transactions on Energy Conversion*, Vol. 15, No. 3, 354-360, 2000.

Chan, C. C. and Y. S. Wong, Electric vehicles charge forward, *Power and Energy Magazine, IEEE*, Vol. 2, No. 6, 24-33, 2004.

Chan, C. C., E. W. C. Lo, and W. X. Shen, The overview

of battery technology in electric vehicles, *Proceedings of International Electric Vehicle Symposium*, CD-ROM, 1999.

Chan, C. C., The state of the art of electric and hybrid vehicles, *Proceedings of IEEE*, Vol. 90, No. 2, 245-275, 2002.

Chiasson, J. and B. Vairamohan, Estimating the state of charge of a battery, *IEEE Transactions on control systems technology*, Vol. 13, No. 3, 465-470, 2005.

Karden, E., S. Buller, and R. W. D. Conchker, A frequency-domain approach to dynamical modeling of electrochemical power sources, *Electrochimica Acta 47*, 2347-2356, 2002.

Karden, E., P. Mauracher, and A. Lohner, Battery management system for energy efficient battery operation: strategy and practical experience, *Proceedings of International Electric Vehicle Symposium*, 91-98, 1996.

Lin, C. T. and C. S. G. Lee, *Neural Fuzzy Systems*, Prentice-Hall, 1996.

Qi, G. G., J. M. Li, and H. Hang, A new battery state of charge indicator for electric vehicles, *Proceedings of International Electric Vehicle Symposium*, 631-635, 1996.

Song, S. K. and K. H. Kim, A dynamic state of charge model for electric vehicle batteries, *Proceedings of International Electric Vehicle Symposium*, 519-527, 1994.

Tenno, A., R. Tenno, and T. Suntio, Battery impedance and its relationship to battery characteristics, *Twenty fourth Annual International Telecommunications Energy Conference*, 176- 183, 2002.

Yamazaki, T., K. Sakurai, and K. I. Muramoto, Estimation of the residual capacity of sealed lead-acid batteries by neural network, *Proceedings of International Telecommunication Energy Conference*, 210-214, 1998.

Zhu, C.B., M. Coleman, and W. G. Hurley, State of charge determination in a lead-acid battery: combined EMF estimation and Ah-balance approach, *Thirty fifth Annual IEEE Power Electronic Specialists Conference*, 1908-1914, 2004.

(Received December 7, 2005; accepted February 7, 2006)